Available online at www.sciencedirect.com
ScienceDirect
Journal of Microbiological Methods 67 (2006) 273–280
Journal of Microbiological Methods
www.elsevier.com/locate/jmicmeth

Rapid characterization of microbial biodegradation pathways by FT-IR spectroscopy

Wei E. Huang [a,b,*], David Hopper [b], Royston Goodacre [c], Manfred Beckmann [b], Andrew Singer [a], John Draper [b]

[a] *Molecular Microbial Ecology Laboratory, CEH-Oxford, Mansfield Road, Oxford. OX1 3SR, UK*
[b] *Institute of Biological Sciences, University of Wales, Aberystwyth, SY23 3DA, UK*
[c] *Chemistry Department, UMIST, Manchester, M60 1QD, UK*

Received 1 December 2005; received in revised form 3 April 2006; accepted 3 April 2006
Available online 5 June 2006

Abstract

Fourier transform-infrared (FT-IR) spectroscopy has become an important tool for rapid analysis of complex biological samples. The infrared absorbance spectrum could be regarded as a "fingerprint" which is characteristic of biochemical substances. In this study, *Pseudomonas putida* NCIMB 9869 was grown with either 3,5-xylenol or *m*-cresol as the sole carbon source, each inducing different metabolic pathways for *m*-cresol biotransformation. FT-IR spectroscopy was capable of differentiating both induced cultures of *P. putida* NCIMB 9869 as well as the resulting biotransformation product mixtures. FT-IR spectral analysis indicated that carboxylic acids were key chemicals responsible for distinguishing the products of the two catabolic pathways. Gas chromatography–mass spectrometry (GC-MS) was performed to validate the FT-IR analysis, indicating that two carboxylic acids, 3-hydroxybenzoic acid and 2,5-dihydroxybenzoic acid, were present as *m*-cresol biotransformation products from 3,5-xylenol-grown cells, but were absent in *m*-cresol-grown cells. The ability to use FT-IR to rapidly distinguish between biotransformation product mixtures as well as differentially induced bacterial strains suggests this approach might be a valuable tool for screening large biotransformation assays for novel products and metabolic mutants.

Keywords: FT-IR; Metabolic profile; Classification; Biodegradation; Pathway; Genetic algorithm; *Pseudomonas putida* NCIMB 9869

1. Introduction

Biological metabolites are usually associated with biological functions, enzymes, and gene expressions (Goodacre et al., 2004). Analysis techniques have been developed to measure biological metabolites such as, GC-MS (gas chromatography–mass spectrometry), LC-MS (liquid chromatography–mass spectrometry) and NMR (nuclear magnetic resonance) (for a review, please see Fiehn, 2001). However, many of these techniques are best suited for in-depth analysis of only a few biological samples due to their capital, labour and time costs. In this light, there is a niche for the development of a rapid, inexpensive high-throughput technique that provides sufficient interrogative power to distinguish bacterial strains on a genetic, phenotypic and/or metabolic level. In recent years, vibrational spectroscopies such as Fourier transform infrared (FT-IR) (Goodacre et al., 2000, 1998; Oberreuter et al., 2002) and Raman spectroscopy (Huang

* Corresponding author. Molecular Microbial Ecology Laboratory, CEH-Oxford, Mansfield Road, Oxford. OX1 3SR, UK. Tel.: +44 1865 281685; fax: +44 1865 281696.
E-mail address: whu@ceh.ac.uk (W.E. Huang).

0167-7012/$ - see front matter © 2006 Elsevier B.V. All rights reserved.
doi:10.1016/j.mimet.2006.04.009

et al., 2004; Jarvis and Goodacre, 2004a,b; Maquelin et al., 2002a, 2000; Schuster et al., 2000a,b; Singer et al., 2005) have been developed for analysing many characteristics of microbiological samples. Raman spectroscopy has been developed into a powerful tool for DNA, protein and bacterial classification analysis. However, the approach is still not a sufficiently high throughput as compared with Fourier transform infrared spectroscopy (FT-IR).

FT-IR spectroscopy measures vibrations of functional groups of chemicals. The advantages of this system are minimal sample preparation, as well as being rapid, non-invasive, accurate, automated, inexpensive and quantitative. The absorbance spectrum generated by FT-IR can be used to identify specific chemical features and can be used as a 'fingerprint' for mixed, complex samples. FT-IR spectroscopy has been demonstrated to be an effective tool for interrogating bacterial strains (Goodacre et al., 2000, 1998). However, its efficacy in differentiating metabolic changes of differentially induced bacteria or genetically identical bacterial strains on different growth substrates remains untested.

In this paper we investigate the ability of FT-IR to distinguish two different *m*-cresol metabolic pathways in *Pseudomonas putida* NCIMB 9869 after growth on 3,5-xylenol or *m*-cresol (Hopper and Kemp, 1980; Jain et al., 1991). After growth on 3,5-xylenol, *P. putida* NCIMB 9869 metabolises *m*-cresol via *m*-hydroxybenzoate following the gentisate pathway (Hopper and Taylor, 1975). However, after growth on *m*-cresol, the bacterium metabolises *m*-cresol via 3-methylcatechol, which is further metabolised through the catechol pathway via *meta*-fission (Fig. 1, re-drawn based on Hopper and Taylor, 1975). The FT-IR spectral fingerprint was used to identify key chemical moieties in the biotransformation products that distinguish the two metabolic pathways. GC-MS was carried out to validate the FT-IR analysis.

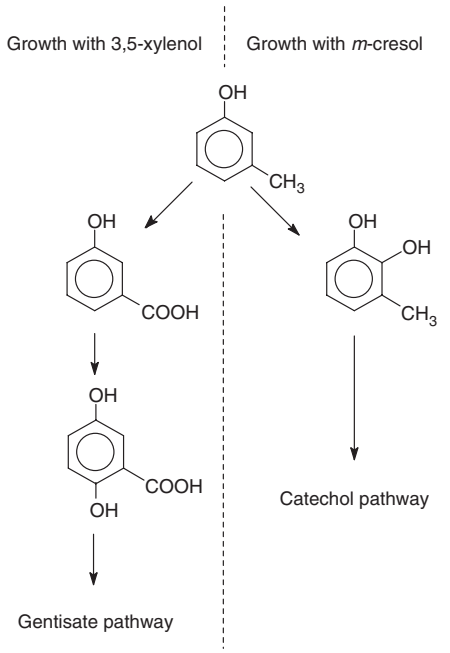

Fig. 1. Different pathways for metabolism of *m*-cresol. After growing with 3,5-xylenol or *m*-cresol, *P. putida* NCIMB 9869 uses the gentisate or catechol pathways for oxidising *m*-cresol (Hopper and Taylor, 1975).

In addition, FT-IR also examined three genetically distinct bacterial strains (*Escherichia coli* DH5α, *P. putida* NCIMB 9816, *Acinetobacter* sp. (ADP1 and green fluorescent protein (GFP)-labelled ADP1-21GF; Huang et al., 2005a). The ability to use FT-IR to rapidly distinguish between biotransformation product mixtures as well as differentially induced bacterial strains without interference from GFP-labelling suggests this approach might be a valuable tool for screening large biotransformation assays for novel products as well as metabolic mutants.

2. Materials and methods

2.1. Strains and growth conditions

The six bacterial strains used in this study were *E. coli* DH5α, *P. putida* NCIMB 9816 (Cane and Williams, 1982), *Acinetobacter* sp. ADP1 (Juni and Janik, 1969) and *Acinetobacter* sp. ADP1-21GF (a GFP gene was inserted into *are*C region (Huang et al., 2005a)), which were grown in 100-ml Luria-Bertani (LB) medium. *P. putida* NCIMB 9869 was grown in medium containing per litre, Na_2HPO_4, 4.33 g; KH_2PO_4, 2.65 g; NH_4Cl, salts solution (Hopper and Taylor, 1975), 4.0 ml; and either *m*-cresol (0.03% w/v) or 3,5-xylenol (0.03% w/v) as sole carbon source. *P. putida* NCIMB 9816, *Acinetobacter* sp. ADP1 and *Acinetobacter* sp. ADP1-21GF were grown for 16 h at 28 °C and *E. coli* DH5α at 37 °C. *P. putida* NCIMB 9869 was grown for 16 h at 30 °C. Each strain was prepared in quadruplicate. Cells were harvested by centrifugation at 3000 rpm, for 10 min, and washed three times with 0.85% NaCl and resuspended in 0.85% NaCl achieving 10^9 cells/ml before FT-IR measurement.

2.2. Oxidation of m-cresol by P. putida NCIMB 9869

P. putida NCIMB 9869 biodegrades *m*-cresol via *m*-hydroxybenzoate after growth on 3,5-xylenol, following the gentisate pathway (Hopper and Taylor, 1975). However, after growth on *m*-cresol, the bacterium metabolises *m*-cresol via 3-methylcatechol, which is further

metabolised through the catechol pathway via *meta*-fission (Fig. 1).

One hundred-milliliter cultures of *P. putida* NCIMB 9869 were grown with *m*-cresol (0.03% w/v) or 3,5-xylenol (0.03% w/v) as the sole carbon source. Five replicates of each treatment were performed. Stationary-phase cultures were harvested by centrifugation (12000×*g* for 10 min) and each resuspended in 2 ml of 42 mM phosphate buffer, pH 7.0. The 3,5-xylenol grown suspensions contained about 4.2 mg cells dry wt./ml and the *m*-cresol grown culture about 6 mg cells dry wt./ml. These cultures were used to oxidize *m*-cresol at 30 °C in a conventional Warburg apparatus. The flasks contained 1.6 ml cell suspension (in phosphate buffer solution), 0.2 ml 20% (w/v) KOH and 0.2 ml of 20 mM *m*-cresol. At the point where oxygen uptake plateaued (slope approaches zero, Fig. 3), cells were removed by centrifugation and the supernatant filtered (0.2 μm filter); the filtrate was analysed by FT-IR. Each sample was run eight times.

2.3. FT-IR analysis of bacterial strains

Analysis of each bacterial strain and metabolite filtrate sample was performed (Goodacre et al., 2000, 1998) by adding a 10 μl sample into a 100-well aluminium plate in quadruplicate. Before analysis, samples were dried in an oven at 50 °C oven for 30 min. FT-IR analysis was performed using a Bruker IFS28 FT-IR spectrometer equipped with a mercury–cadmium–telluride detector cooled with liquid N_2. Spectrums were collected with Opus software (version 2.1), using a scan range of 4000–600 cm^{-1} and a resolution of 4 cm^{-1}; each spectrum was represented by 882 points.

2.4. Cluster analysis

ASCII data were imported into Matlab version 6.1 (The MathWorks, Inc., 24 Prime Par Way, Natick, MA, USA) and normalised with the smallest absorbance set to 0 and the highest to +1 for each spectrum. Principal components analysis (PCA; Jolliffe, 1986) was employed to reduce the dimensionality of the FT-IR data from 882 to 20 principal components (PCs) (>99% of the total explained variance). Discriminant function analysis (DFA; Manly, 1994) separated groups based on these retained PCs and the a priori knowledge of which spectra were replicates, a process that does not bias the analysis. DFA was performed to maximize between-group variance and minimize within-group variance. To validate discrimination performed by DFA, projection analysis was employed to project test data to PCA space and DFA space generated by the training set. Briefly, PC-DFA was carried out as detailed above, randomly chosen test FT-IR spectra, which were not used in the construction of the PC-DFA model, were mathematically projected first into PCA space and then into DFA space generated by the training set (Jarvis and Goodacre, 2004a,b).

The key bands contributing to DFA classifications were recovered by inspection of PC-DFA loadings ranking or genetic algorithm (GA)-DFA analysis (Jarvis and Goodacre, 2004a,b). These variables were used to re-perform DFA analysis and the data would be considered validated if the re-plotted PC-DFA was the same as in the previous PC-DFA analysis. The most discriminatory bands for DFA classification were recovered, and DFA analyses were re-performed for classification by using 11 or 15 of 882 most contributed bands.

2.5. Gas chromatography analysis

One hundred-microliter filtrates were dried by vacuum extraction (DNA speed Vac, DNA 120, Savant Co.) and resuspended in 50 μl methanol for analysis by gas chromatography–mass spectroscopy (GC-MS) measurement. Derivatization of dried extracts was achieved by protecting the carbonyl moieties by methoximation using 100 μl of a 20 mg ml^{-1} solution of methoxyamine hydrochloride (Fluka) in pyridine (Fluka) at 30 °C for 90 min. Acidic protons were subsequently derivatized with 100 μl *N*-methyl-*N*-trimethylsilyltrifluoride (MSTFA, M and N) at 37 °C for 30 min. Samples of 2 μl of the extracts were injected into a GC-MS system consisting of a Focus autosampler (ATAS), an Agilent 6890N gas chromatograph and a Leco Pegasus III Time-of-Flight detector. Injection temperature was 250 °C, the interface was set to 260 °C and the ion source was adjusted to 230 °C. Helium flow was 1 ml min^{-1}. After 5 min at 80 °C, oven temperature was increased by 60 °C min^{-1} to 330 °C, held at 330 °C for 5 min and cooled to 80 °C. Peak finding was performed using ChromaTof software (Leco). Salicylic acid in samples was quantified using a three-point calibration of standard solutions prepared and analysed accordingly.

3. Results and discussion

3.1. Bacterial strains classification by FT-IR analysis

Six bacterial strains, *E. coli* DH5α, *P. putida* NCIMB 9816, *Acinetobacter* sp. ADP1 and its mutant *Acinetobacter* sp. ADP1-21GF and *P. putida* NCIMB 9869, were measured by FT-IR after growth in the described conditions. Statistical analysis of projection PC-DFA was applied to the classification with the results plotted in Fig. 2A. To validate the DFA analysis 12 spectra of

each bacterium were used as a training data set to construct a classification system and 4 independent spectra were used as the test set. Each test set clustered amongst the data present within its training set, thus validating the groupings observed (Fig. 2A). The first discriminant function (DF1) indicates the highest variation and DF2 demonstrates the second highest variation. The testing data were all correctly allocated into their training clusters and therefore validated the classification. Fig. 2A shows that four different strains (*E. coli* DH5α, *P. putida* NCIMB 9816, *Acinetobacter* sp. and *P. putida* NCIMB 9869) were clustered at four different positions on DF1. *Acinetobacter* sp. ADP1 and ADP1-21GF also closely clustered (Fig. 2A), reinforcing the fact that they are of the same genus and species, differing only in that ADPW21-GF is engineered with a constitutively expressed GFP (Huang et al., 2005a). The tight clustering of these strain variants indicates that GFP expression does not lead to significant changes in the FT-IR profile, presumably because the laser scan wavelengths of FT-IR are in the infrared region. Moreover, the tight clustering of these strain variants indicates that GFP expression does not lead to significant changes in the FT-IR profile, presumably because the FT-IR laser scan wavelengths (infrared region) could not excite the GFP protein.

Although *P. putida* NCIMB 9869 and *P. putida* NC IMB 9816 are closely related strains, their large separation indicates growth media might have significant

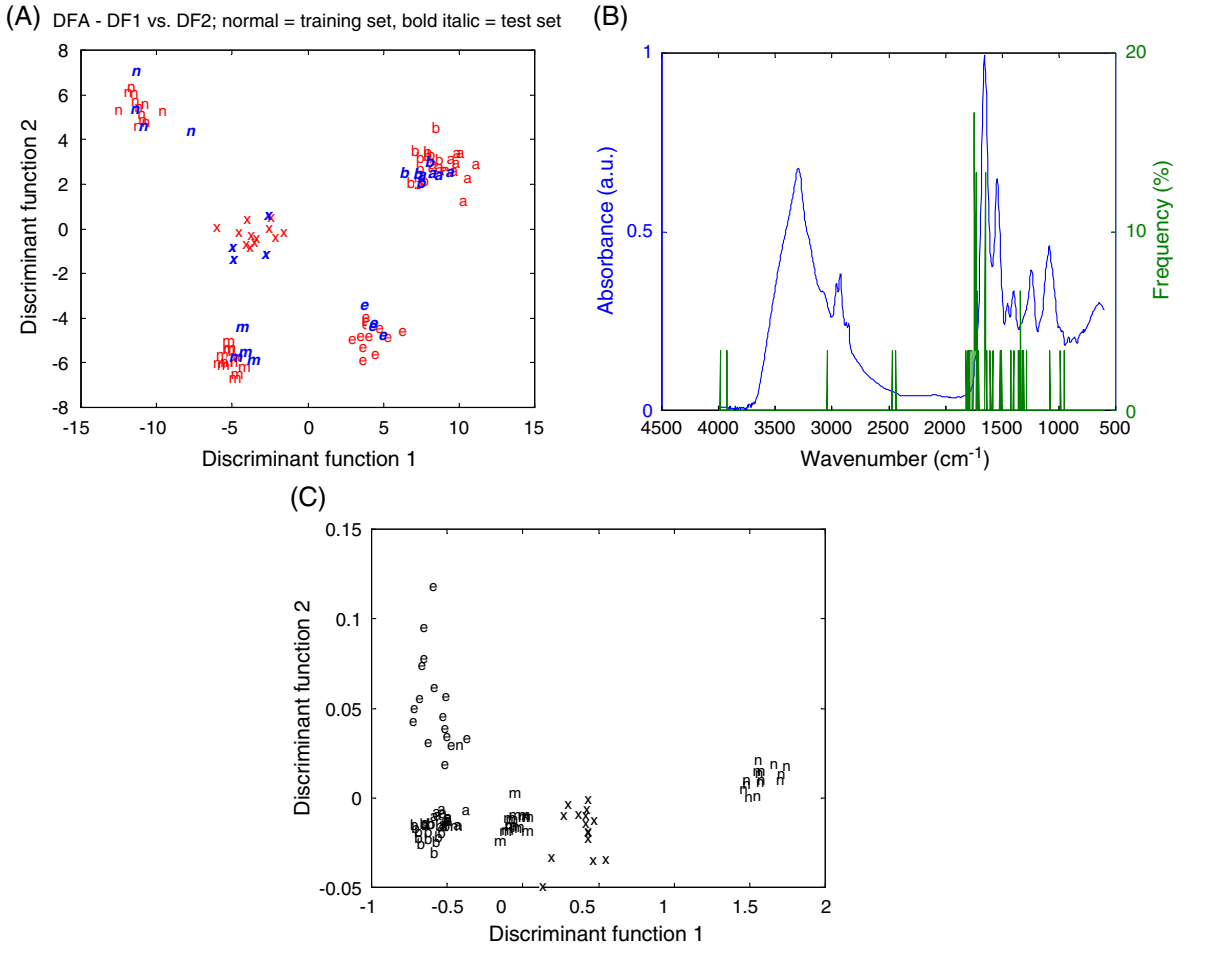

Fig. 2. Bacterial FT-IR classification. (A) DFA classification with cross-validation based on FT-IR bacterial measurements. It shows the relationship between the six bacterial samples. Normal letters represent training set and italic bold represent independent test set. (B) Most frequent FT-IR variables were selected from 100 independent GA-DFA runs. The higher frequency lines, the more significant bands responsible for the DFA classification. (C) DFA plot only based on 11 most contributed bands (1747–1728, 1689–1685, 1666, 1643, 1631 cm^{-1}) which are derived from Table 1. Bacteria are coded as follows; *P. putida* NCIMB 9869 growth *m*-cresol (m), *P. putida* NCIMB 9869 growth with 3,5-xylenol (x), *E.* coli DH5α (e), *P. putida* NCIMB 9816, (n), *Acinetobacter* sp. ADP1 (a), and *Acinetobacter* sp. ADP1-21GF (b).

Table 1
Putative assignments of some bands most contributed for bacteria classification

DF top loadings (cm^{-1})	Most frequently selected wavenumbers (cm^{-1}) by genetic algorithm	Assignment (Coates, 2000; Maquelin et al., 2002b)
DF1		
1740	1740	>C═O str of esters
1736	1736	>C═O str of esters
1743	1743	C═O stretch from amide I region
1747	1747	C═O stretch from amide I region
1732	1732	>C═O str of esters
1632		Amide I of β-pleated sheet structures
1666	1666	Alkenyl C═C stretch
1643	1643	Alkenyl C═C stretch
1728	1728	>C═O str of esters
1018		Cyclohexane ring vibrations
1022		Cyclohexane ring vibrations
DF2		
1685		Amide I band components resulting from antiparallel pleated sheets and β-turns of proteins
1701		Amide I band components resulting from antiparallel pleated sheets and β-turns of proteins
1736		>C═O stretch of esters
1697		Amide I band components resulting from antiparallel pleated sheets and β-turns of proteins amide I band
1690		Amide I band components resulting from antiparallel pleated sheets and β-turns of proteins
957		Aromatic C–H in-plane bend
960		Aromatic C–H in-plane bend
1693		Amide I band components resulting from antiparallel pleated sheets and β-turns of proteins
953		Aromatic C–H in-plane bend

effects on bacterial FT-IR spectra (Fig. 2A). Of particular note, *P. putida* NCIMB 9869 growing in *m*-cresol (0.03% w/v) and 3,5-xylenol were positioned closely against DF1 but differently against DF2, suggesting that the growth medium induced the synthesis of different enzyme systems and led to the changes of bacterial metabolic profiles (Hopper and Taylor, 1975) which were distinguishable by FT-IR.

Key bands contributing to DFA classification in Fig. 2A were identified by examining PC-DFA loadings and carrying out 100 independent GA (genetic algorithm)-DFA analysis. The recovered bands by PC-DFA loading ranking and genetic algorithm (GA)-DFA analysis (Jarvis and Goodacre, 2004a,b) were compared and the results are listed in Table 1 along with their biological relevance. The frequently selected bands of GA-DFA runs are shown in Fig. 2B. Both DFA loading and GA-DFA analyses indicate similar key bands which represent mostly fatty acids and proteins responsible for classification (Table 1). Among these key bands, interestingly, 1747 cm^{-1} was also extracted as key for classification of urinary tract isolates (Goodacre et al., 1998; Jarvis and Goodacre, 2005). Using 11 (1747–1728, 1689–1685, 1666, 1643, 1631 cm^{-1}) of 882 bands extracted from these DFA loadings and GA-DFA analyses, a new DFA classification was plotted (Fig. 2C) further emphasizing the relevance of these bands in differentiating the six bacterial strains.

Variations in gene expression could lead to changes in bacterial metabolic profiles. Since FT-IR is measuring

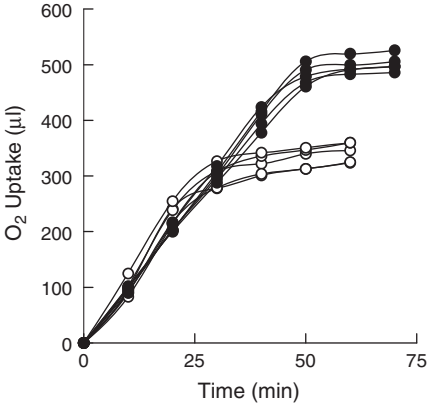

Fig. 3. The oxidation of *m*-cresol by *P. putida* grown on *m*-cresol (○) or 3,5-xylenol (●). The uptake for the endogenous flask has been subtracted in each case.

chemical fingerprints, it could be insensitive to the GFP protein but sensitive enough to differentiate the bacteria with subtle metabolic changes. Hence, FT-IR could be potentially used as a rapid tool to screen for metabolic pathway mutants.

3.2. Oxidation of and classification of different m-cresol catabolic pathways

Some biodegradation genes are induced by metabolites of the parent compounds, for example, operons of naphthalene or other polycyclic aromatic hydrocarbons are usually activated by salicylate or phthalate, rather than naphthalene (King et al., 1990; Mahaffey et al., 1988). Presumably, bacteria could release some water-soluble metabolites or inducers to rapidly induce and activate degradation operons of their sibling cells. Intermediate metabolites are often detectable in the aqueous phase during degradation (Huang et al., 2005b). It has been reported that 3-hydroxybenzoic acid and 2,5-dihydroxybenzoic acid can accumulate in media as well as induce catabolic pathways (Feng et al., 1999; Zhao et al., 2004, 2005).

Complete oxidation of *m*-cresol by whole cells of *m*-cresol-grown *P. putida* NCIMB 9869 was achieved in 30 min, whereas 3,5-xylenol-grown cells required 46 min (Fig. 3). GC-MS analysis indicated that 3-hydroxybenzoic acid and 2,5-dihydroxybenzoic acid (gentisic acid) were present in cell-free solution after 3,5-xylenol-grown cells oxidized *m*-cresol, but were absent in assays carried out by *m*-cresol-grown cells (data not shown). This is in good agreement with the *m*-cresol

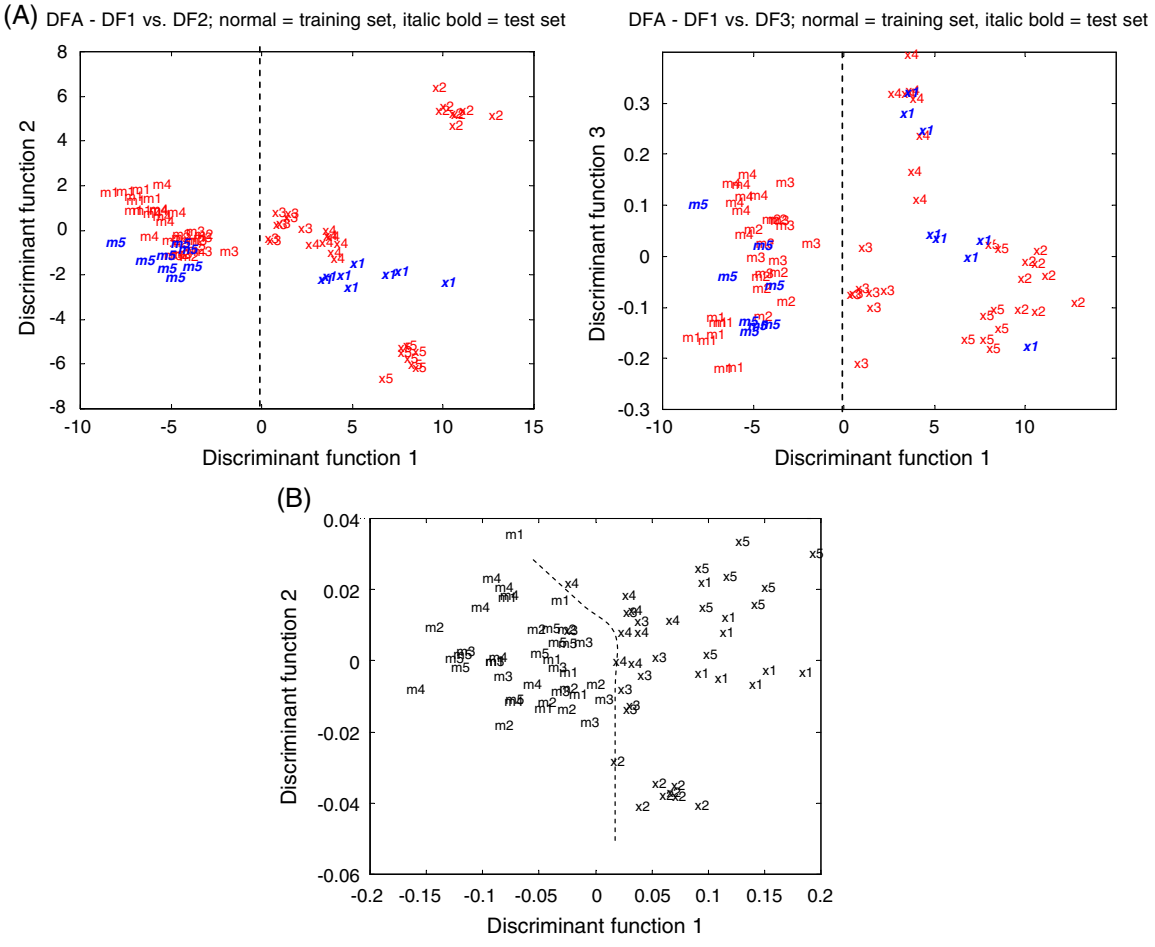

Fig. 4. FT-IR metabolic classification. (A) DFA classification with cross-validation based on FT-IR data. Normal letters represent training set and italic bold represent independent test set. (B) DFA plot only based on the most contributed 15 bands (1558–1573, 1461–1469, 1365–1388 cm^{-1}) which are derived from Table 2. Samples are coded as follows; *P. putida* NCIMB 9869 grown with 3,5-xylenol uses the gentisate pathway for *m*-cresol oxidization (x); when grown with *m*-cresol, it uses the catechol pathway for *m*-cresol oxidization (m). The numbers represent each of the five replicates of experiments.

Table 2
Putative assignments of some bands most contributed for metabolites classification

DF1 top loadings, wavenumbers (cm^{-1})	Assignment (Coates, 2000)
1562	Carboxylic acid
1566	Carboxylic acid
1558	Carboxylic acid
1570	Carboxylic acid
1454	Aromatic ring stretch
1377	Carboxylic acid
1470	Aromatic ring stretch
1381	Carboxylic acid
1373	Carboxylic acid
1466	Aromatic ring stretch
1473	Aromatic ring stretch
1369	Carboxylic acid
1462	Aromatic ring stretch
1385	Carboxylic acid
1389	Carboxylic acid

oxidization pathways of *P. putida* NCIMB 9869 shown in Fig. 1.

The differentially induced cells, representing the two pathways of *m*-cresol oxidization were clearly separated by DFA (Fig. 4A) and the testing data all correctly allocated into their training clusters validating the classification. Greater variation was seen in the results for 3,5-xylenol-grown cells than for *m*-cresol-grown cells. This might be explained by the fact that *m*-cresol induces the catechol rather than the gentisate pathway (Fig. 1). The induction of another active metabolic pathway in 3,5-xylenol-grown cells might have introduced some variations between samples, whereas no such metabolic shift occurred in the *m*-cresol-grown cells. DFA loadings of Fig. 4A were inspected and 15 bands, detailed in Table 2, were determined to contribute most significantly to the differentiation, most notably the aromatic ring and carboxylic acid moieties. These moieties are consistent with the induced pathway of *P. putida* NCIMB 9869 (Fig. 1).

The gentisate pathway generates both 3-hydroxybenzoic acid and 2,5-dihydroxybenzoic acid (Fig. 1), whereas the catechol pathway generates 3-methylcatechol (Fig. 1). GC-MS data indicates that both biotransformation product mixtures contained sugar-like compounds, but traces of 3-hydroxybenzoic acid and 2,5-dihydroxybenzoic acid were only present in the medium of 3,5-xylenol-grown cells after oxidation of *m*-cresol, thereby confirming the expression of the gentisate pathway. 3-Methylcatechol was not detected as a product of *m*-cresol biodegradation by *m*-cresol-grown cells.

Since PC-DFA loading ranking and GA-DFA generated consistent results (Table 1), we only used PC-DFA loading ranking to recover key FT-IR bands (Table 2). GC-MS analysis was in good agreement with FT-IR analysis which showed that bands of carboxylic acids and aromatic rings were responsible for the difference between the two pathways (Table 2). To validate the significance of these bands, 15 bands of carboxylic acids and aromatic rings (1558–1573, 1461–1469, 1365–1388 cm^{-1}) from a total of 882 bands were taken out and re-analyzed. The two oxidization pathways can be differentiated by PCA. A bi-PCA is plotted in Fig. 4B confirmed the significance of these bands.

In conclusion, FT-IR spectral fingerprints were shown to differentiate metabolic pathways of *m*-cresol within the same bacterial strain. Statistical analysis has identified that carboxylic acid was a key chemical moiety differentiating the products of the two pathways. GC-MS validated the FT-IR analysis suggesting that the carboxylic acids 3-hydroxybenzoic acid and 2,5-dihydroxybenzoic acid were the chemical products unique to the 3,5-xylenol-grown cell biotransformation. Hence, FT-IR might provide a rapid, non-destructive, cost-effective approach for assessing the production of novel chemicals in complex matrices.

Acknowledgments

We are grateful to Dr. Roger Jarvis of the University of Manchester who provided the GA code and advice for statistical analysis. We also thank Professor Peter Williams of the University of Wales Bangor who kindly provided *P. putida* NCIMB 9816.

References

Cane, P.A., Williams, P.A., 1982. The plasmid-coded metabolism of naphthalene and 2-methylnaphthalene in *Pseudomonas* strains—phenotypic changes correlated with structural modification of the plasmid Pww60-1. Journal of General Microbiology 128, 2281–2290.

Coates, J., 2000. Encyclopedia of analytical chemistry. John Wiley and Sons Ltd, Chichester.

Feng, Y.M., Khoo, H.E., Poh, C.L., 1999. Purification and characterization of gentisate 1,2-dioxygenases from *Pseudomonas alcaligenes* NCIB 9867 and *Pseudomonas putida* NCIB 9869. Applied and Environmental Microbiology 65, 946–950.

Fiehn, O., 2001. Combining genomics, metabolome analysis, and biochemical modelling to understand metabolic networks. Comparative and Functional Genomics 2, 155–168.

Goodacre, R., Timmins, E.M., Burton, R., Kaderbhai, N., Woodward, A.M., Kell, D.B., Rooney, P.J., 1998. Rapid identification of urinary tract infection bacteria using hyperspectral whole-organism fingerprinting and artificial neural networks. Microbiology–UK 144, 1157–1170.

Goodacre, R., Shann, B., Gilbert, R.J., Timmins, E.M., McGovern, A.C., Alsberg, B.K., Kell, D.B., Logan, N.A., 2000. Detection of the dipicolinic acid biomarker in *Bacillus* spores using Curie-point pyrolysis mass spectrometry and Fourier transform infrared spectroscopy. Analytical Chemistry 72, 119–127.

Goodacre, R., Vaidyanathan, S., Dunn, W.B., Harrigan, G.G., Kell, D.B., 2004. Metabolomics by numbers: acquiring and understanding global metabolite data. Trends in Biotechnology 22, 245–252.

Hopper, D.J., Taylor, D.G., 1975. Pathways for the degradation of *m*-cresol and *p*-cresol by *Pseudomonas putida*. Journal of Bacteriology 122, 1–6.

Hopper, D.J., Kemp, P.D., 1980. Regulation of enzymes of the 3,5-xylenol-degradative pathway in *Pseudomonas putida*: evidence for a plasmid. Journal of Bacteriology 142, 21–26.

Huang, W.E., Griffiths, R.I., Thompson, I.P., Bailey, M.J., Whiteley, A.S., 2004. Raman microscopic analysis of single microbial cells. Analytical Chemistry 76, 4452–4458.

Huang, W.E., Goodacre, R., Elliott, G.N., Beckmann, M., Worgan, H., Bailey, M.J., Williams, P.A., Scullion, J., Draper, J., 2005a. The use of chemical profiling for monitoring metabolic changes in artificial soil slurries caused by horizontal gene transfer. Metabolomics 1, 305–315.

Huang, W.E., Wang, H., Huang, L.F., Zheng, H.J., Singer, A.C., Thompson, I.P., Whiteley, A.S., 2005b. Chromosomally located gene fusions constructed in *Acinetobacter* sp. ADP1 for the environmental detection of salicylate. Environmental Microbiology 7, 1339–1348.

Jain, R.K., Bayly, R.C., Skurray, R.A., 1991. Specific deletion of a large segment of pRA500-A 3,5-xylenol degradative plasmid. Letters in Applied Microbiology 12, 216–220.

Jarvis, R.M., Goodacre, R., 2004a. Discrimination of bacteria using surface-enhanced Raman spectroscopy. Analytical Chemistry 76, 40–47.

Jarvis, R.M., Goodacre, R., 2004b. Ultra-violet resonance Raman spectroscopy for the rapid discrimination of urinary tract infection bacteria. FEMS Microbiology Letters 232, 127–132.

Jarvis, R.M., Goodacre, R., 2005. Genetic algorithm optimization for pre-processing and variable selection of spectroscopic data. Bioinformatics 21, 860–868.

Jolliffe, I.T., 1986. Principal component analysis. Springer, New York.

Juni, E., Janik, A., 1969. Transformation of *Acinetobacter calcoaceticus* (*Bacterium anitratum*). Journal of Bacteriology 98, 281–288.

King, J.M.H., Digrazia, P.M., Applegate, B., Burlage, R., Sanseverino, J., Dunbar, P., Larimer, F., Sayler, G.S., 1990. Rapid, sensitive bioluminescent reporter technology for naphthalene exposure and biodegradation. Science 249, 778–781.

Mahaffey, W.R., Gibson, D.T., Cerniglia, C.E., 1988. Bacterial oxidation of chemical carcinogens—formation of polycyclic aromatic-acids from benz-*a*-anthracene. Applied and Environmental Microbiology 54, 2415–2423.

Manly, B.F.J., 1994. Multivariate statistical methods: a primer. Chapman and Hall, London.

Maquelin, K., Choo-Smith, L.P., van Vreeswijk, T., Endtz, H.P., Smith, B., Bennett, R., Bruining, H.A., Puppels, G.J., 2000. Raman spectroscopic method for identification of clinically relevant microorganisms growing on solid culture medium. Analytical Chemistry 72, 12–19.

Maquelin, K., Choo-Smith, L.P., Endtz, H.P., Bruining, H.A., Puppels, G.J., 2002a. Rapid identification of *Candida* species by confocal Raman micro-spectroscopy. Journal of Clinical Microbiology 40, 594–600.

Maquelin, K., Kirschner, C., Choo-Smith, L.P., van den Braak, N., Endtz, H.P., Naumann, D., Puppels, G.J., 2002b. Identification of medically relevant microorganisms by vibrational spectroscopy. Journal of Microbiological Methods 51, 255–271.

Oberreuter, H., Charzinski, J., Scherer, S., 2002. Intraspecific diversity of *Brevibacterium linens*, *Corynebacterium glutamicum* and *Rhodococcus erythropolis* based on partial 16S rDNA sequence analysis and Fourier-transform infrared (FT-IR) spectroscopy. Microbiology-Sgm 148, 1523–1532.

Schuster, K.C., Reese, I., Urlaub, E., Gapes, J.R., Lendl, B., 2000a. Multidimensional information on the chemical composition of single bacterial cells by confocal Raman microspectroscopy. Analytical Chemistry 72, 5529–5534.

Schuster, K.C., Urlaub, E., Gapes, J.R., 2000b. Single-cell analysis of bacteria by Raman microscopy: spectral information on the chemical composition of cells and on the heterogeneity in a culture. Journal of Microbiological Methods 42, 29–38.

Singer, A.C., Huang, W.E., Helm, J., Thompson, I.P., 2005. Insight into pollutant bioavailability and toxicity through Raman confocal microscopy. Journal of Microbiological Methods 60, 417–422.

Zhao, B., Yeo, C.C., Lee, C.C., Geng, A., Chew, F.T., Poh, C.L., 2004. Proteome analysis of gentisate-induced response in *Pseudomonas alcaligenes* NCIB 9867. Proteomics 4, 2028–2036.

Zhao, B., Yeo, C.C., Poh, C.L., 2005. Proteome investigation of the global regulatory role of sigma(54) in response to gentisate induction in *Pseudomonas alcaligenes* NCIMB 9867. Proteomics 5, 1868–1876.